IEEE Access
Multidisciplinary | Rapid Review | Open Access Journal

Received August 25, 2019, accepted September 2, 2019, date of publication September 10, 2019,
date of current version September 24, 2019.

Digital Object Identifier 10.1109/ACCESS.2019.2940648

A Key Performance Indicator to Assess the Frequency Stability of Wind Generation Dominated Power System

ELYAS RAKHSHANI[1], (Member, IEEE), DIGVIJAY GUSAIN[1], VINAY SEWDIEN[1,2], JOSÉ L. RUEDA TORRES[1], (Senior Member, IEEE), AND MART A. M. M. VAN DER MEIJDEN[1,2], (Member, IEEE)

[1]Department of Electrical Sustainable Energy, Delft University of Technology (TUD), 2628 Delft, The Netherlands
[2]TenneT TSO B.V., 6800 Arnhem, The Netherlands

Corresponding author: Elyas Rakhshani (rakhshani@ieee.org)

ABSTRACT High penetration of power electronic interfaced generation, like wind power, has an essential impact on the inertia of the interconnected power system. It can pose a significant threat to the frequency stability. This paper introduces the notion of the key performance indicator (KPI) and illustrates its application on large scale power systems, including Fast Frequency Response (FFR) and a high share of wind power, to measure the possible distance to the frequency stability limit. The proposed KPI estimates the change of frequency performance (e,g., ROCOF, NADIR) in the frequency containment period. The effect of FFR is analyzed by introducing a droop based controller for wind power plants. The FFR controller responds to a drop in grid frequency with a temporary increase of the wind active power. The proposed KPI maps a change in key system variables (e.g., system kinetic energy, aggregated generation output) onto the change of frequency performance. A comprehensive analysis using DIgSILENT, Matlab, and Python is performed for GB reduced size system. According to the obtained results, the FFR capability of wind generator leads to improvements of NADIR especially in cases with high penetration levels of wind power. The proposed KPI is a valuable tool for the frequency stability assessment in power system planning studies. It can be determined based on off-line simulations, and it can assist the system operators for frequency stability assessment in intra-day operational planning.

INDEX TERMS Frequency stability, fast frequency response, inertia emulation, MIGRATE, power system stability indicator, wind power integration.

I. INTRODUCTION

As indicated in the European Commission energy roadmap, the increase of renewable-based generation identified as one of the main components of the EU's energy de-carbonization policy [1], [2]. Thus, in the next years, more power electronics (PE) will be applied to interconnect load, storage, and Renewable Energy Sources (RES) to the electrical transmission network. As PE interfaced generation (PEIG) and power electronic interfaced load (PEIL) behave differently than conventional generation and load, it is of importance to study the possible impact of increasing amounts of PE on the stability performance of the power system. In this regard, different aspects of power system stability issues have been investigated for transient stability [3], [4], voltage [5], [6] and frequency stability [7], [9], and in most of those research works, possible violation of technical limits to ensure stable operation in high share of PEIG has been acknowledged [8].

The research work presented in this paper is one of the outcomes of the first work package of the (Massive InteGRATion of power Electronics) MIGRATE project [10], which addresses power system stability issues of transmission grids under high penetration of PE. According to Transmission System Operators (TSOs) of the MIGRATE consortium and other members of the European Network of

The associate editor coordinating the review of this manuscript and approving it for publication was Siqi Bu.

Transmission System Operators for Electricity (ENTSO-E), frequency stability ranked among the main topics of concern [10]–[13].

Reduction of inertia, as a consequence of the displacement of conventional generations with PEIGs, decreases the robustness of the system against active power imbalances and frequency variations [14], [15]. The study of frequency stability indicators and identification of the distance to the frequency stability limit (i.e., threshold defined by TSO, e.g., 250 mHz/s for rate-of-change-of-frequency - ROCOF) is a challenging task, considering the high diversity of operating conditions caused by the stochastic nature of demand and renewables. Most of the recent research on assessment of frequency stability is devoted to the analysis of a single or a few selected worst-case of operational scenarios [16], [17]. Nevertheless, a systematic approach for defining a distance to instability is needed to accurately characterize the relational pattern between a stability indicator (e.g., rate-of-change-of-frequency, ROCOF or NADIR) and key system variables (e.g. kinetic energy). This paper tackles this gap by performing an extended analysis with different levels of share (penetration) of PEIG.

Given the above, the following are the main contributions of this paper: The first contribution is related to the proposition of a key performance indicator (KPI) and its testing on a synthetic model of the Great Britain (GB) system. The goal is to evaluate the distance to the threshold of acceptable dynamic frequency performance (e.g. in terms of ROCOF and NADIR) in power systems with high penetration of PEIG. The KPI shows how the system can move towards the threshold as a consequence of changes in a key variable (e.g. kinetic energy). The consideration of the sum of maximum active power deviation as an additional key variable is proposed for tackling the problem of having different values of frequency stability indicator (ROCOF, NADIR) for the same value of the first key variable (i.e., kinetic energy).

The second contribution is related to the application of the KPI to evaluate of the impact of the FFR capability added into the model of wind generators (WGs) used for the numerical simulations shown in this paper. Furthermore, a systematic procedure for implementing the KPI in the control room for assisting the system operator with situational awareness is suggested. According to this procedure, for a given dispatch with a given loading condition, from defined relational curves, the system operator can estimate the corresponding values of ROCOF/NADIR with respect to the thresholds defined in grid code requirements.

Lastly, in order to see the effects of different level of wind power penetration, the GB test system is also used for testing the proposed KPI in a case with 65% penetration of wind power generation. In the studied GB system, operational scenarios, named as Gone Green (GG), for years 2020 and 2030 are derived based on ten years planning perspective [18].

The remainder of the paper is as follows: Section II presents a brief review of widely used frequency stability indicators. The used power system models and the wind generator (WG) control structure with incorporating the concept of FFR for the participation of WG in the frequency control are presented in Section III. Section IV focuses on the definition of the KPI and its implementation. While the proposed methodology for calculation of the KPI is presented in Section V. In Section VI, the application of the KPI on the GB test system is presented. Section VII is devoted to a recommendation for using the KPI in the control room. Finally, concluding remarks are summarized in Section VIII.

II. REVIEW OF FREQUENCY STABILITY INDICATORS

A. FREQUENCY STABILITY INDICATORS

ROCOF and NADIR are the most widely used indicators to assess the frequency performance in the frequency containment period [19], [20]. ROCOF corresponds with the frequency gradient after an active power imbalance [21]. The ROCOF is defined as shown in (1):

$$\mathrm{ROCOF(t)} = \frac{\mathrm{df(t)}}{\mathrm{dt}} \tag{1}$$

where f stands for frequency (in Hz). For a synchronous generator, the derivative of the frequency, df/dt, can be determined from the per-unit formulation of its swing equation [22], that is

$$\frac{\mathrm{df(t)}}{\mathrm{dt}} = \frac{\frac{\Delta P(t)}{\mathrm{S_{B-i}}}}{2\mathrm{H_i}}\mathrm{f_0} = \frac{\frac{\Delta P(t)}{\mathrm{S_{B-i}}}}{\mathrm{T_{N-i}}}\mathrm{f_0} \tag{2}$$

where ΔP is the change of the active power (e.g. amount of MW lost due to a generator outage),$\mathrm{f_0}$ is the nominal frequency in Hz, $\mathrm{H_i}$ is the inertia constant of the generator in seconds, and $\mathrm{T_{N-i}}$ is the acceleration time constant (time in seconds taken to accelerate a generator from standstill to nominal speed – which requires nominal torque applied to the shaft). $\mathrm{S_{B-i}}$ is the nominal apparent power of the generator (in MVA) [23]. The subscript i denotes i-th generator among n generators in the system.

The relationship between the kinetic energy stored in the rotating masses (MW·s),$\mathrm{E_{kin-i}}$, at nominal speed and the inertia constant $\mathrm{H_i}$ of a synchronous generator is defined by equation (3) [24]-[25].

$$\mathrm{E_{kin-i}} = \mathrm{H_i} \cdot \mathrm{S_{B-i}} \tag{3}$$

The total kinetic energy of the system is computed by using equation (4) [25].

$$\mathrm{E_{kin-sys}} = \sum_{\mathrm{i=1}}^{\mathrm{n}} \mathrm{E_{kin-i}} \tag{4}$$

where n is the number of synchronous generators in the system.

Equation (5) is determined by substituting equation (3) into (2). It can be seen that the ROCOF is inversely proportional to the kinetic energy (as it does with the inertia constant in equation (2)).

$$\frac{\mathrm{df(t)}}{\mathrm{dt}} = \frac{\Delta P(t)}{2 \cdot \mathrm{E_{kin-i}}}\mathrm{f_0} \tag{5}$$

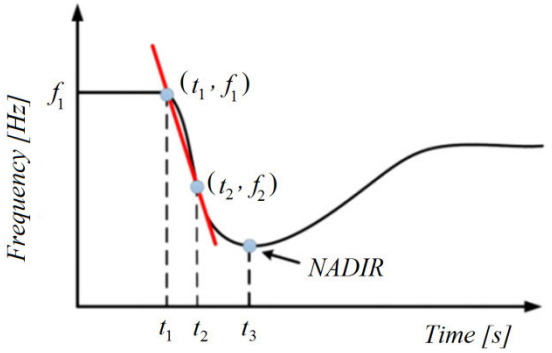

FIGURE 1. Illustration of the required points for ROCOF computation. NADIR is highlighted.

Motivated by equation (5), an approximation of ROCOF, as shown in equation (6) is suggested in [26] and [27] for qualitative assessment of the frequency performance within the time window of the system inertial response.

$$\mathrm{ROCOF(t)} = \frac{\Delta P_{\mathrm{sys}}(\mathrm{t})}{2\left(\mathrm{E_{kin-sys}} - \mathrm{E_{kin-lost}}\right)}\mathrm{f_0} \tag{6}$$

where ΔP_{sys} and $\mathrm{E_{kin-lost}}$ stand for change in system active power and kinetic energy lost, for instance, due to the sudden disconnection of a generator, respectively. For a multi-machine system, an equivalent generating unit is defined to represent the average behavior of n synchronous units. The equivalent generating unit is known in existing literature as Centre of Inertia (COI). According to [28], the frequency of the COI is defined as:

$$\mathrm{f_{COI}\,(t)} = \frac{\sum_{\mathrm{i=1}}^{\mathrm{n}} \mathrm{H_i S_{B-i} f_i(t)}}{\sum_{\mathrm{i=1}}^{\mathrm{n}} \mathrm{H_i S_{B-i}}} \tag{7}$$

where $\mathrm{f_i(t)}$ is the time-frequency response of the i-th generator, recorded for a given time window.

The ROCOF is estimated from the frequency of the COI, by considering a time window of 500 ms following the disturbance [28]. The initial value at $\mathrm{t_1}$ and the value at $\mathrm{t_2}$ are used for calculation of ROCOF. It is worth to recall that the analysis done in this study focuses on the assessment of the frequency performance in the containment period, time window of the inertial response of synchronous generators. Thus, in such conditions, the ROCOF is calculated as follows:

a) Compute the frequency Centre Of Inertia (COI) for the system/area according to equation (7) [28].
b) Get the time of the event ($\mathrm{t_1}$) as the initial value of ROCOF for calculation. See Figure 1 for a graphical illustration.
c) Find the index of an intermediate time $\mathrm{t_2}$ such that, for instance, $\mathrm{t_2} = \mathrm{t_1}+0.5$ s.
d) Make a linear fitting to $\mathrm{f_{COI}(t)}$ in $\mathrm{t} \in [\mathrm{t_1}, \mathrm{t_2}]$.
e) Get the slope of the linear function as ROCOF.

The normative contingencies for the interconnected operation in Continental Europe, as defined by ENTSO-E in [20] and [21] for the ROCOF computation, are the tripping of the largest generation units or loss of big industrial loads. For example, in the GB system, the loss of pump storage units when pumping, which behaves as the largest system demand loss, could raise the frequency and lead to a potential ROCOF event [29]. Furthermore, the loss of interconnectors could also trigger a ROCOF event (analogous effect as observed in generation loss or demand loss). The maximum value of ROCOF allowed in the Great Britain system is 125 mHz/s, whereas for the continental Europe values between 500 mHz/s and 1 Hz/s have been recorded [20]. The NADIR indicator corresponds with the lower frequency value obtained after a power imbalance, which depends on the system inertia, the response of the available frequency containment reserves, settings of a primary frequency control system, the size and location of the disturbance, and the pre-disturbance operating conditions [30].

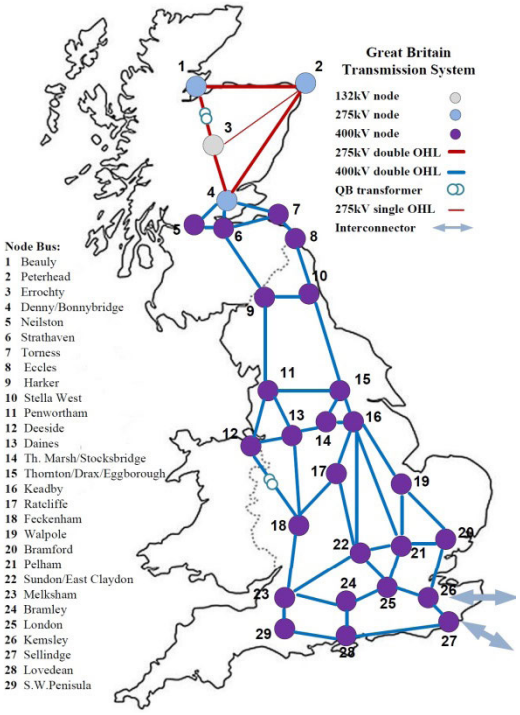

FIGURE 2. Great Britain reduced transmission system (from [31]).

The criterion that defines the limit for NADIR is expressed as ($\mathrm{f_{Nadir}} \geq \mathrm{f_{min}}$). In this criterion, $\mathrm{f_{min}}$ is the minimum acceptable frequency defined in a grid code. This indicator has high relevance in the frequency control because a low value (lower than 47.5 Hz) might lead to uncontrolled frequency excursions [21].

In order to avoid load shedding, the maximum frequency deviation is defined as +/−800 mHz in continental Europe as stated in sections A-D2.3 and A-D2.4 of [20], which represents a NADIR threshold of 49.2 Hz.

III. SYSTEM MODELLING

A. GB TEST SYSTEM

The synthetic model of the GB system used in this paper is based on the reduced size model presented in [18] and [31]. The main structure of the network is shown in Figure 2,

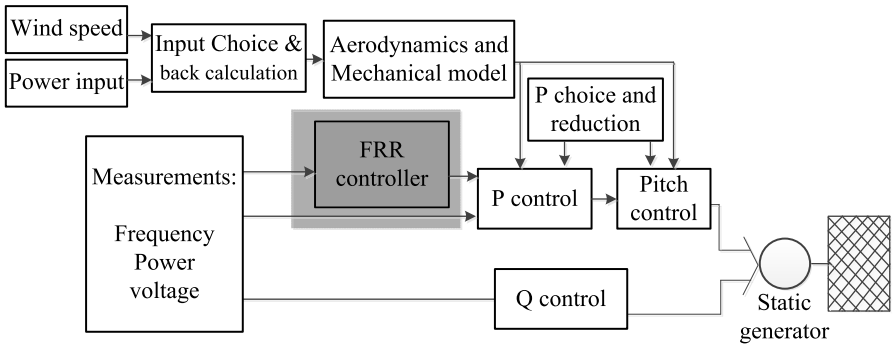

FIGURE 3. Block diagram showing the overall structure of the WG controller.

where each of the 29 substations represents a grouped level of generation, load demand, and grid losses.

For the implementation of future scenarios in the GB system, it was chosen to select the most extreme, Gone Green transition scenario (defined based on the expansion plans of GB system [18]), in order to study the highest level of wind power migration.

The Gone Green scenario is based on the assumption that renewable generation and environmental targets are achieved: 15% of all energy from RES by 2020, and 80% reduction in greenhouse gasses by 2050. The studied scenarios in this paper are the baseline scenario in 2016 with penetration up to 15%, Gone Green scenario in 2020 (GG2020) with penetration up to 40% and the Gone Green scenario in 2030 (GG2030) with penetration up to 78%.

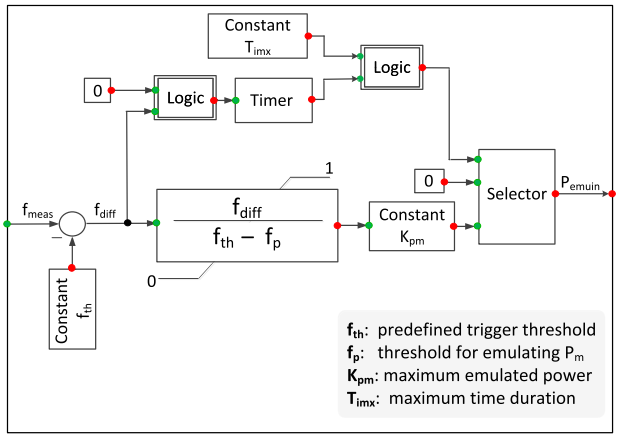

FIGURE 4. Implemented FFR block of the wind power controller.

B. WIND GENERATOR MODEL

The WG model was built based on the standard IEC 61400-27 series from [13]. A list of the blocks that represent additions to the IEC standard and a short description of their main functions is also shown in Figure 3, which can be used as a reference for the overall structure of the WG (type 4) [13].

The main features of the model are described as follows:

- In the measurement part of this model, the blocks Frequency, Power, and Voltage measurements are connected directly to the terminals of the WG. These measurement values and the currents from the Generator Block are used for initializing the model.
- The Generator block contains the PowerFactory element ''Static Generator'', and works as a current source. The Generator block is set according to IEC 61400-27-1 [32].
- The mechanical part is represented by the Aerodynamic block, which calculates the mechanical power of the turbine, and the mechanical block, which contains a single mass model based on IEC 61400-27-1 [32].
- Input part: there is a block which gives the wind speed. It must contain an external file with wind speed measurement data in m/s. As an alternative to wind speed, the maximal available power can be used as an input by using a Power input block. In the Input choice and back-calculation block, one of the two input options can be chosen.
- In the control part, the block P control and Pitch angle controller are taken from [33]. The block named ''FFR controller'', shown in Figure 3, also constitutes an addition to the WG model. Its output is also added to the active power reference value when the FFR controller is activated.

In this paper, for adding the capability of FFR to the model of WG, a specific droop based controller is designed. The general structure of the proposed FFR controller is presented in Figure 4. It constitutes a droop based fast active power injection controller, which is implemented inside of the FFR block (highlighted with light grey in Figure 3) of the WG model. The input signal of the droop based controller is the frequency deviation, and its output is the additional power that is added to the active power reference of the wind turbine controller. The energy for this additional power is drawn from the rotating masses of the WG.

The activation process is based on a comparator (cf. Fig. 4). The trigger signal will be generated by comparing the measured frequency (f_{meas}, measured in Hz) against a predefined trigger threshold (f_{th}, expressed in Hz). The controller is activated when f_{meas} equals f_{th}. In this study, the value of f_{th}

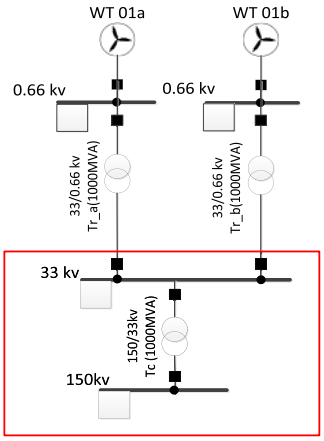

FIGURE 5. Grid interface of a wind park with two types of WGs.

is assumed to be equal to 49.85 Hz. In case the frequency reaches an even lower value, corresponding with a second threshold f_p, then, the maximal allowed power through emulated power is released. There is a linear dependency (defined by a proportional gain K_{pm}) between frequency deviation and the additional power signal (P_{emuin}). The following calculation is performed:

$$P_{emuin}(t) = \frac{f_{th} - f_{meas}(t)}{f_{th} - f_p} K_{pm} \tag{8}$$

According to [11] and [13], the value of the gain K_{pm} can be set up to 25% of the nominal WG active power. Therefore, according to the logic presented in Figure 4, if the frequency rises above f_{th} or if the maximal allowed time for FFR (T_{imx}) is exceeded, then the output of the controller, P_{emuin}, is set to zero again.

The maximal allowed time is calculated according to the logic shown in the upper loop of the controller illustrated in Figure 4. The user can input a constant to define the value of T_{imx}. Then, by using a timer and selector blocks (cf. Figure 4), the output of the controller can be switch to zero if T_{imx} is reached.

According to [11] and [13], T_{imx} can be set in the range of 5s - 15s. The selected value of T_{imx} shall consider the time of occurrence of the first peak of the frequency increase/decrease after the occurrence of an imbalance and the response time of the available source of energy (like additional storage in DC link of the WG type 4 or available fast-acting reserves) for frequency containment. A wind park is used to represent the connection of several feeders with WGs as depicted in Figure 5.

An important difference in the software-based model between the WP and WG is that, in the WP, the active and reactive powers are controlled at the Point of Common Coupling (PCC) and not at the terminals of the WG. The general structure of the wind park control used in PowerFactory is shown in Figure 6. The blocks Power measurement, Frequency measurement, and Voltage measurement are connected to the PCC. Hence, the external files that are inserted in P set-point WP, X set-point WP and Cosphi set-point WP give reference values for the PCC [33].

IV. THE NOTION OF KPI FOR FREQUENCY STABILITY ASSESSMENT

As explained in Section II, the stability indicators (ROCOF and NADIR) are widely used for assessing the dynamic frequency performance within the frequency containment period. Nevertheless, considering the challenges from reduced inertia and variable active power output of PEIG, a simple tool is needed to estimate the value of ROCOF/NADIR under different operating conditions (defined by different load demand levels, system inertia levels, and disturbances that cause active power imbalance). As reported in several studies by utilities [34], it is possible to define a mapping curve, that is, a single-valued relationship between a frequency stability indicator (ROCOF/NADIR) and a key system variable (commonly defined in terms of inertia or kinetic energy). Such a mapping curve is presented in Fig. 7, which illustrates that the operator can infer a value of the frequency stability indicator for a given value of the key system variable. In that way, if an operational action that results in a change of the key system variable (e.g. reduction of inertia due to displacement of synchronous generators in a conventional power plant by a wind power plant) occurs, the operator can determine the new value of the frequency stability indicator and its distance from a threshold defined in grid code requirements.

An illustrative example is presented in Figure 8 to highlight the value of a mapping curve for estimating the distance to the threshold for frequency stability. As shown in Figure 8, different mapping curves (illustrated with continuous black lines) might be used to evaluate the frequency performance in the containment period when considering different system loading conditions.

Different operational statuses (emergency, alert, normal) are also illustrated in Figure 8. In this example, the width of the illustrated statuses corresponds with the allowed values of ROCOF/NADIR. Two sample operating conditions are shown in Figure 8. The first one, denoted by OC1, corresponds with a case in which the system will have an unacceptable value of ROCOF/NADIR (emergency status) due to low kinetic energy in the system. The mapping curve MC1 shows how the ROCOF can be brought to an acceptable value (normal status) when the necessary level of kinetic energy is reached. By contrast, the second sample operating condition, OC2 point in mapping curve MC2, shows how ROCOF/NADIR will degrade when there is a reduction of the level of kinetic energy.

As reported in [2], multiple values of the frequency stability indicator may be associated with the same value of key system variable. This issue happens when the loading of the system changes, while the key system variable remains unchanged. To overcome this drawback, a complementary mapping curve with a new key system variable is proposed in this paper. The complementary mapping curve will be used

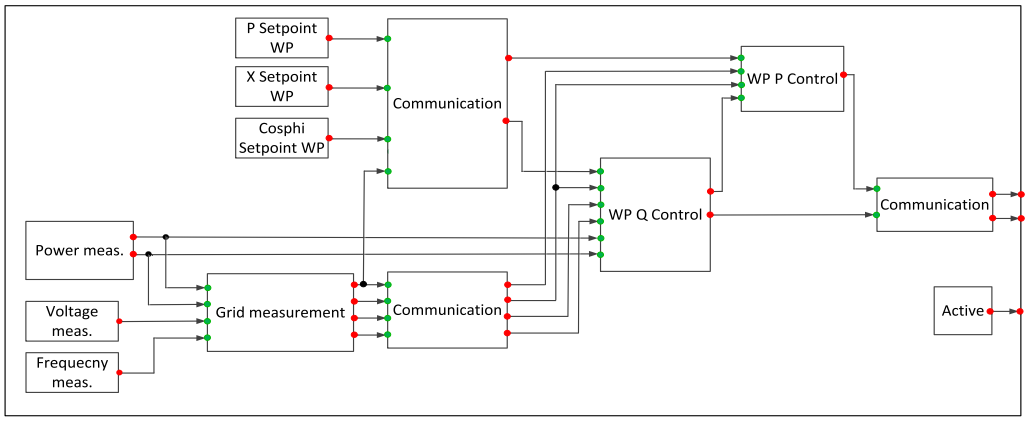

FIGURE 6. Structure of WP controller in DIgSILENT.

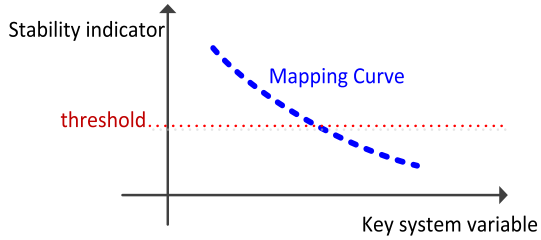

FIGURE 7. KPI for frequency stability assessment: Estimation of distance to stability limits from a mapping curve (single-valued relationship).

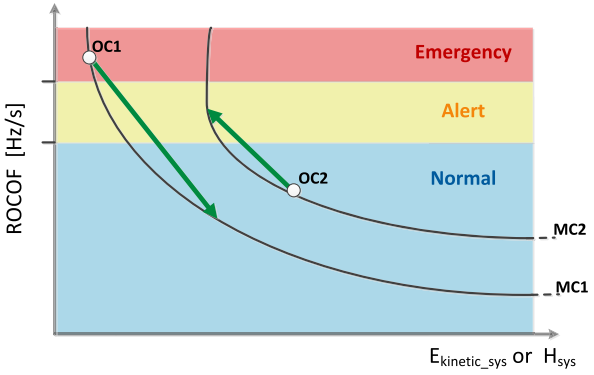

FIGURE 8. Example of frequency stability assessment based on mapping curves.

to help the system operator to obtain a single value of the frequency stability indicator when dealing with the assessment of frequency stability in different loading conditions and considering the same range for different values of the first key system variable (i.e. kinetic energy).

The necessity of having a complementary mapping curve is elaborated by considering the example presented in Figure 8. As shown in this figure, there might be a situation in which different mapping curves are available to consider different system loading conditions and disturbances. In such a situation, the mapping between the stability indicator (ROCOF/NADIR) and kinetic energy as the key system variable will not be lead to a unique value for ROCOF/NADIR.

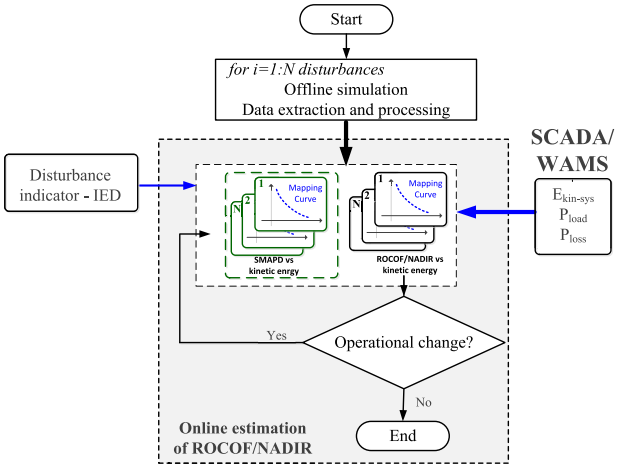

FIGURE 9. Implementation of the proposed frequency stability KPI in a control room (IED stands for the intelligent electronic device).

Hence, an additional mapping curve shall be defined to help the operator to decide which mapping curve (MC1 or MC2) should be chosen. The consideration of the Sum of Maximum Active Power Deviation (SMAPD) as an additional key system variable is proposed for tackling this issue.

The use of two mapping curves is illustrated in the application example shown in Figure 9. For instance, if a (fossil fuel-fired) generator displacement is planned for a given loading condition, then, the user can directly estimate the value of ROCOF/NADIR from the first mapping curve (ROCOF/NADIR vs Kinetic Energy). In case of having different values of ROCOF/NADIR for two different loading conditions, but with the same level of kinetic energy, the second mapping curve (SMAPD vs. Kinectic Energy) as a complementary mapping should be checked by the user to choose the right value of ROCOF/NADIR corresponding to each loading condition. The mapping curves are determined based on offline simulations. Nevertheless, as shown in Figure 9, they can be used in combination with measurements from the Energy Management System (EMS) to assist situational

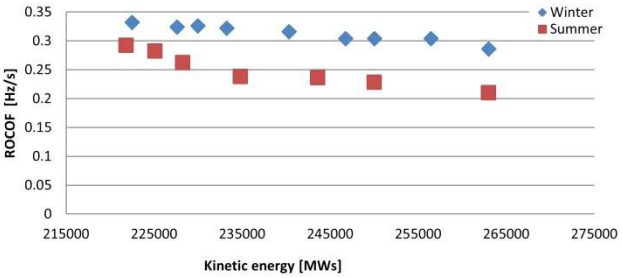

FIGURE 10. ROCOF vs. kinetic energy for GG2020.

awareness in the control room. The calculation procedure for determining the mapping curves is presented in Section V.

In the final part of this section, the rationale behind the selection of the new key system variable is discussed based on an analysis to reflect the implications of system active power load demand and losses. In the analysis, the GB test system (Figure 2) is used.

In the test system, the GG scenario has been taken into account to capture the effects of the high share of wind power [31]. For the sake of comparison, the same range of kinetic energy and the same disturbance are considered for winter and summer peak demands of GG2020 (Gone Green 2020 scenario). In both loading conditions, a generator outage (G11 in the North England area), which entails approximately around 6% of total generation, is considered. This disturbance occurs at $t = 26$ s, and the simulation time is 36 s. For the sake of comparative illustration, the ROCOF values, for different loading profiles in winter and summer are summarized in Figure 10. The value of ROCOF for the same kinetic energy level is more critical in higher loading conditions (i.e., higher load demand in winter results in higher ROCOF). This shows that the impact of active power load demand on the frequency performance cannot be ignored and it is a reasonable assumption to take into account the variation of active power load demand of the system as one of the key system variables used in the complementary mapping of the proposed KPI. This observation is in agreement with what is reported by [12].

Thus, load characteristics like voltage or frequency dependency and its residual impacts have to be considered for having a more confident assessment of frequency stability performance [12].

As it is well known, the total electrical power provided by the generators in a system must be equal to the total electrical power demand consumed by the network. This includes the electrical loads together with all the losses in the transmission network. Any change in this equilibrium that disrupts the steady-state operation of the power system is considered as a power imbalance which leads the generators to decelerate, exciting an oscillatory behaviour [35], [36]. The current in the transmission network also oscillates with the same frequency as the generators. The current through a particular transmission element causes ohmic losses, which are part of the consumed power. This issue might be more

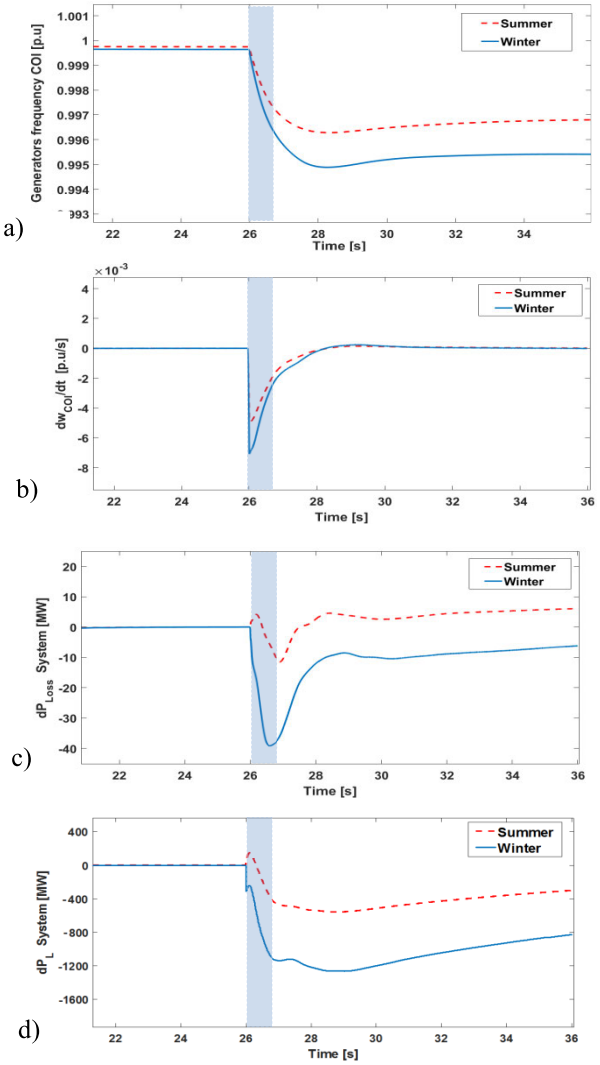

FIGURE 11. System performance for GG2020: (a) frequency of the COI for GG2020 with G11 outage at 26 s; (b) time derivative of the frequency of the COI; (c) variation of grid losses over time [MW]; (d) variation of the active power demand respect to its value before the fault.

significant if a considerable amount of wind power, around 65%, is replaced by conventional synchronous generators. Therefore, the variation of grid losses during an imbalance can also be considered another key system variable which can help to understand the frequency performance in the containment period. These losses can be obtained from the state estimator available in the EMS of each control room considering SCADA/synchrophasor measurements technologies [37], [38]. This aspect becomes clearer considering the results are shown in Figure 11. To capture the time variation of the grid losses, two scenarios from GG2020, for winter and summer, with the same disturbance are considered.

In Figure 11a, the frequency of the COI is depicted for winter and summer profiles, whereas the time derivative of the frequency of the COI and the time variation of power losses are in Figure 11b and Figure 11c. The time derivative of the frequency of the COI (shown in Figure 11b) is determined

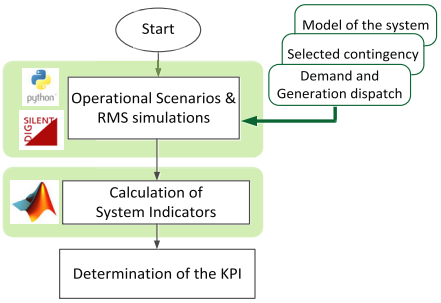

FIGURE 12. The overall methodological procedure.

by applying the derivative term of the frequency of the COI (shown in Figure 11a).

Note that when the derivative of the frequency of the COI changes abruptly due to the imbalance, a similar pattern occurs for the ohmic losses. This finding is in agreement with what was proven in [36], i.e. fluctuations of the frequency of the COI are dictated by the oscillations in the transmission network's ohmic losses.

A similar relational pattern occurs with the time variation of active power demand, as shown in Fig. 11(d). Hence, the SMAPD is computed as the sum of the total active power load demand deviation and total active power losses deviation determined at t = 0.5 s from the time of occurrence of an imbalance and computed w.r.t. their values in pre-disturbance condition. This time frame corresponds with the period in which ROCOF is determined.

$$SMAPD = \Delta P_{L,max,sys}\big|_{0.5s} + \Delta P_{Loss,sys}\big|_{0.5s} \qquad (9)$$

where $\Delta P_{L,max,sys}$ is the maximum value of the active power deviations in the system/area and $\Delta P_{Loss,sys}$ is the deviations in system losses after the occurrence of a fault. The complementary mapping curve has kinetic energy vs SMAPD.

V. THE METHODOLOGY USED FOR SYSTEM INDICATORS

The overall methodological procedure is summarised in Fig. 12. The model of the power system, the components' data, load demand, generation dispatches, and selected disturbance are the necessary inputs for KPI calculation. The procedure starts with the generation of different operational scenarios with different penetration levels of PEIG. For each operational scenario, a dynamic database considering different dispatches for generators with different loading levels is used. For the selected disturbance, the values of ROCOF and NADIR can be estimated through the mapping process explained in the following sub-sections.

A. OPERATIONAL SCENARIOS AND RMS SIMULATION

As shown in Figure 13-a, a set of different generator dispatches cases for the test grid have to be prepared as an Excel file. It should cover the most critical scenarios with different ranges of kinetic energy (i.e., considering not only change of power share, but also disconnection of synchronous generators).

These Excel files are the input data set for a python-PowerFactory interface to call the set of defined dispatches. Then, the power system model is simulated by using DIgSILENT PowerFactory. This software allows an interaction with Python which can be exploited to automate the execution of RMS simulations and data extraction.

Once the database with the generators' frequency response is obtained (time_ DB block in Figure 13b) in the data extraction step, the raw data is migrated to MATLAB to begin the processing in the next step.

B. CALCULATION OF SYSTEM INDICATORS

In this step, Matlab scripts are used to process the data obtained from the RMS simulations in PowerFactory to calculate the system indicators (ROCOF/NADIR) for a different level of kinetic energy. The procedures are schematically shown in Figure 13-b.

The structure of the database is such that there exists one CSV-file per each simulation scenario, for which the entire set of simulations needs to be examined. Each CSV-file has the time series and the corresponding frequency values associated with the dynamic response of each active (i.e., in-service) synchronous generator in the system. Therefore, this information is used to compute the $f_{COI}(t)$, from which the ROCOF is obtained.

C. DETERMINATION OF THE PROPOSED KPI

In this step, the obtained information from previous steps can be used for performing two types of mapping curves for the determination of the KPI. The following steps shall be followed:

1. First mapping curve: Use the computed values of the ROCOF and NADIR (stored as CSV-files as an output of the previous step) for each of the defined dispatches for determining the trend of ROCOF/NADIR vs. the level of system kinetic energy.
2. Second mapping curve: For each dispatch, calculate the Sum of Maximum Active Power Deviation (SMAPD) of load and losses, which is equivalent to the aggregated actual generation output. The SMAPD reflects the effect of the active power consumption in the system on the system active power balance. The trend of SMAPD vs. level of system kinetic energy is determined according to the following procedure:
   - Step1: record the time series (for the considered simulation time window) of the losses and active power demand deviations in the system.
   - Step2: calculate SMAPD. SMAPD is the sum of the maximum values of active power load and grid losses (aggregated system generation output) throughout the power system with respect to their pre-disturbance value (before the occurrence of imbalance). The calculation of the SMAPD can be performed in the same time window of calculation of the ROCOF, i.e., 0.5 sec after the occurrence of the imbalance.

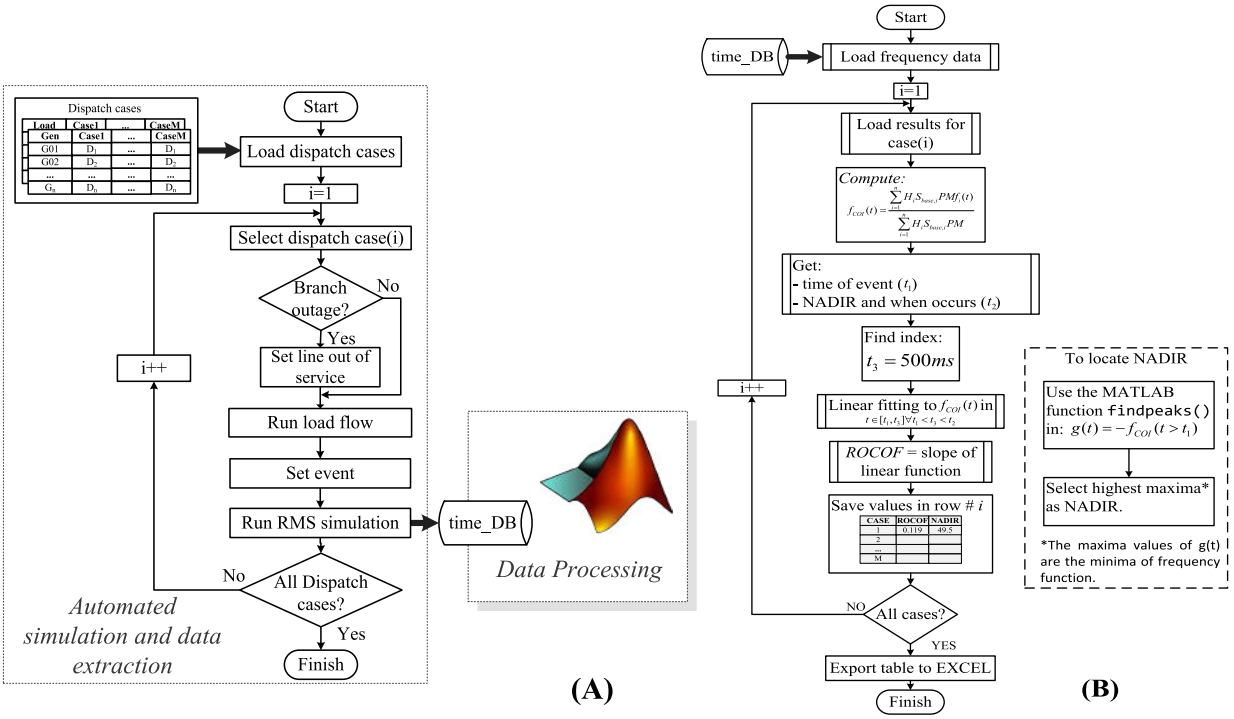

FIGURE 13. A) Procedure for automated simulation and data extraction by combining PowerFactory, Python, and Excel. time_DB stands for a database of time responses of system variables; B) procedure for data processing of frequency response and calculation of ROCOF and NADIR by using Matlab and Microsoft Excel.

- Step3: create the characteristic curve of SMAPD vs. level of system inertia/kinetic energy.

3. Use the obtained mappings from previous steps 2 and 3, to assess the frequency performance in the frequency containment period. In the next section, the proposed KPI is tested and analyzed with the GB system.

VI. TESTING OF THE KPI WITH THE GB TEST SYSTEM

The main results of KPI testing for GB system are presented in this section. The main assumptions that have been taken into account for the KPI for assessment of frequency performance in the containment period are summarised as follows:

- Synchronous generators are the main source of system inertia in the frequency containment period.
- The loads are represented by a constant power model.
- The governors are not optimized to improve ROCOF/NADIR.
- PEIG connected at transmission-level and only WGs type Type-4 are considered. These components do not possess a function for FFR.

The calculation procedure described in Section V has been implemented in the GB test system for different scenarios (2016 as the baseline, GG2020, and GG2030). Analysis for GB system is performed by considering the following conditions:

- Season: Summer, i.e., load peak at 60%.
- Topological change: No.

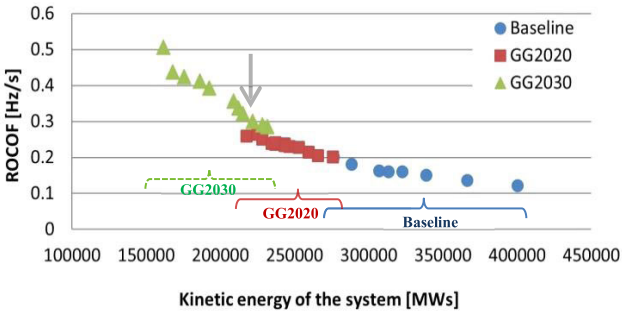

FIGURE 14. Mapping of ROCOF vs. kinetic energy for frequency performance KPI.

- Event: Generator outage (G11 at $t = 26$ s) representing 6% of the total system generation.

As shown in Section V, the main part of the KPI implementation is to obtain the mapping from system kinetic energy into ROCOF/NADIR, which is shown in Figure 14 and Figure 15. Both figures illustrate the values of ROCOF/NADIR that correspond to a set of feasible dispatches covering different wind generation penetration levels.

In Figure 14 and Figure 15, the blue points are related to the baseline scenario which has more synchronous generators with less wind generation (i.e., WG penetration from 5 to 15%), the red values are related to the GG2020 scenario (WG penetration from 15% to 40%) and the green values are related to the GG2030 scenario (60% to 78% of WG penetration).

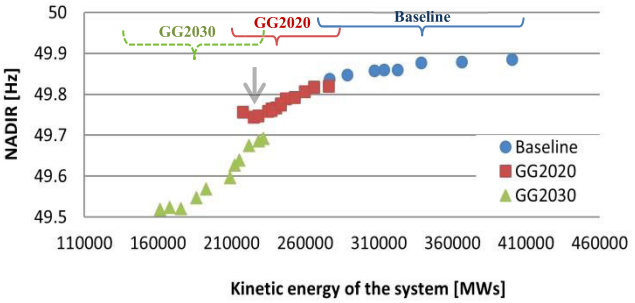

FIGURE 15. Mapping of NADIR vs. kinetic energy for frequency performance KPI.

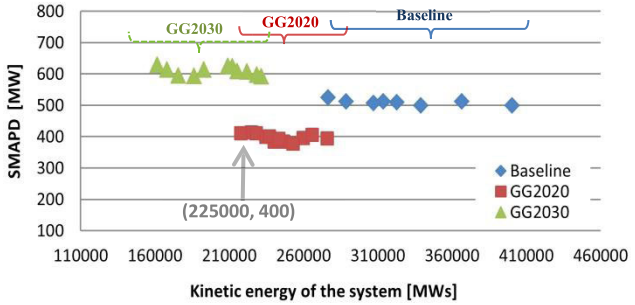

FIGURE 16. SMAPD vs. kinetic energy for frequency performance KPI.

From a simple visual inspection in Figures 14 and 15 of the mapping trends for different scenarios of the GB system, we can observe that the baseline scenario shows a more flat relationship ROCOF/NADIR vs. kinetic energy. Since most of the synchronous generators are in service in the baseline scenario, more variety of feasible kinetic energy is obtained for this case. By contrast, for the year 2020 and 2030, significant changes in ROCOF and NADIR with respect to the kinetic energy level are observed.

As shown in the mapping of Figure 14 and Figure 15, in most of the cases each level of system kinetic energy may be related to a single value of ROCOF/NADIR, but in some cases, two values of ROCOF/NADIR may be associated with the same level of kinetic energy.

The reason behind the difference in ROCOF/NADIR for different loading levels (e.g., winter and summer) is explained in Section IV. For the sake of illustration purposes, if the value of the estimated system kinetic energy is more than 288000 MWs, then, its related value of ROCOF can be estimated directly by the mapping obtained in Figure 14. But, if the value of the system kinetic energy is around 225000 MWs, then, for the same level of system kinetic energy, depending on the system loading (GG2020 or GG2030), different values of ROCOF can be associated. In such a case, additional mapping, shown in Figure 16, from SMAPD helps to choose the right value of ROCOF. The judgment, in this case, is as follows: if the SMAPD is around 400 MW (G2020 scenario in Figure 16) for 225,000 MWs of kinetic energy, then, the estimated value of ROCOF lies in the corresponding loading level (G2020 scenario) in Figure 14.

TABLE 1. Selected parameters for the FFR control block.

Parameter	Value	
f_{th} [Hz]	49.85	Frequency in Hz below which FFR controller will be activated
f_p [Hz]	49.7	The frequency that the maximum emulated power will be released.
f_n [Hz]	50	Nominal frequency
K_{pm} [pu]	0.25	Maximum additional power output from FFR in p.u.
T_{imx} [s]	15	Duration of FFR action

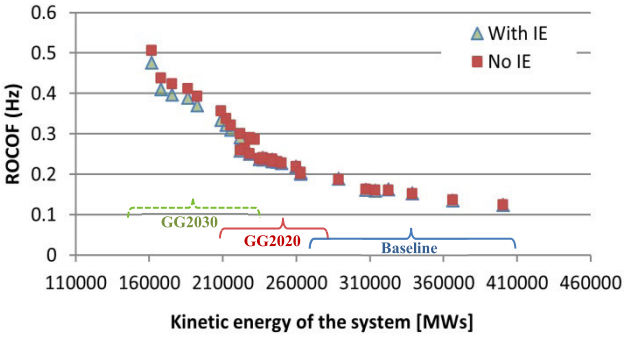

FIGURE 17. Mapping of ROCOF vs. kinetic energy considering inertia emulation of WG.

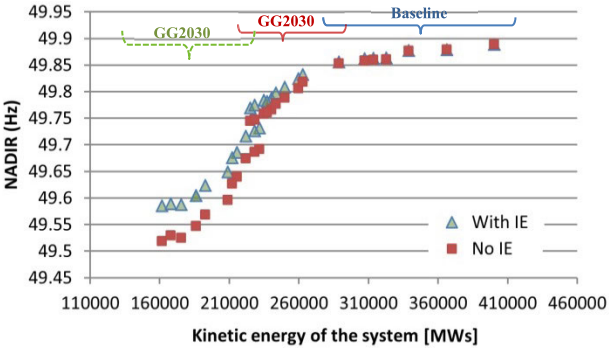

FIGURE 18. Mapping of NADIR vs. kinetic energy considering inertia emulation of WG.

To further analyse the performance of the proposed KPI, more analysis, considering the FFR effect of a WG is performed. The FFR controller is explained in Section VI, and the assumed values for control parameters used for this analysis are presented in Table 1.

The effect of FFR with WG generation for ROCOF and NADIR is presented in Figures 17 and 18, respectively. After repeating the simulations, now considering FFR, the same trends (the relationship between ROCOF/NADIR and Kinetic Energy) are observed as shown in Figures 17 and 18.

By comparing Figures 14 and 15 against Figures17 and 18, from most of the operational scenarios (baseline and GG2020) ROCOF improvements are minor, whereas, for NADIR, the improvements are more appreciable, especially in cases with the higher level of penetration.

This difference in the improvement of ROCOF and NADIR is due to the type of controller and its input signal. As explained in Section VI, the proposed FFR controller is based on a droop control, and the input signal is the deviation of measured frequency itself. Therefore, the main impact of the proposed controller is the improvement in the frequency Nadir. Thus, if the added wind power plants are facilitated by FFR controller, the higher share will result in greater improvements in Nadir. The degree of improvement of Nadir depends on the parameters selected for the controller. For example, choosing a threshold closer to the nominal frequency (e.g., higher than 49.85 Hz) may lead to better values of Nadir due to earlier activation of FFR. A detailed overview of parametric sensitivity analysis is provided in [39].

VII. RECOMMENDATION FOR CONTROL ROOM IMPLEMENTATION

The KPI for the assessment of the frequency performance in the frequency containment period, which is based on mapping curves determined via offline simulations, can be used for the assessment in the control room as illustrated in Figure 9. Note that the figure suggests that mapping curves (ROCOF/NADIR vs. kinetic energy and SMAPD vs. kinetic energy) shall be determined offline, based on a suitable model of the system (i.e., responses obtained via offline simulations have a high resemblance with actual measured responses). For a selected number of disturbances, each one evaluated for a number of dispatches (which entail variation of the power share and system kinetic energy). Thus, a disturbance indicator (e.g. selecting the type of disturbance that actually happens based on an alert signal from protection devices) can be used to select the mapping curves, whereas information (actual kinetic energy, active power demand, active power losses) from the Energy Management System (EMS) is passed through the mapping curves to estimate the ROCOF/NADIR.

It is worth mentioning that System Operators have a well-defined set of credible N-1 contingencies. Furthermore, available accurate forecasts for RES generation, combined with the fact that balance responsible parties have to provide their generation schedule one day in advance to the system operator, results in a fair knowledge of the dispatches in the power system. At last, the network topology can be easily retrieved from the SCADA.

The main limitation of this approach concerns the use of a model implemented in a selected software package. The lack of accuracy of the model to recreate real behaviour can lead to misleading results. Nevertheless, there has been significant progress on model identification from synchrophasor measurements [40]. Thus, the models used by operators can be improved and updated regularly to ensure reliable (from a numerical accuracy point of view) simulation results. Moreover, the computing effort associated with the execution of offline simulations may be of concern for large size systems. Nevertheless, the adoption of high-performance computation in power system simulation software packages can help to significantly reduce the computing time [41], [42]. A reliable estimator of the system kinetic energy is needed. The estimation of total load active power demand and active power losses can be done based on the state estimator, which is usually based on SCADA measurements (1 sample per 2-6 seconds [43]). However, recent proposals have been made to also consider synchrophasor measurements by sampling each 200 to 500 ms [38].

When the proposed KPI is implemented in the control room environment, a prolonged shadow run might be proposed. The goal of the shadow run is to validate and tune the power system model, based on SCADA and PMU data. EirGrid, the Irish TSO, successfully installed a transient stability analysis tool in 2009 that currently runs thousands of simulations within five minutes [44].

VIII. CONCLUSION

This paper presented the notion of KPI for converter dominated power systems to investigate frequency stability performance. The KPI constitutes a way to map the values of a system variable or set of system variables (e.g., kinetic energy) onto the actual value of a stability indicator (e.g., ROCOF, NADIR), thus allowing to estimate the distance to frequency stability limits.

In this study, the GB test system is modified to represent high penetration levels of wind power generation. In the GB system model, different transition scenarios, according to expected development plans, are introduced to consider different levels of wind generation penetrations. Methods to determine the KPIs, based on offline simulations, are proposed. DIgSILENT, Matlab, and Python are used to perform RMS simulations with automated analysis.

For the frequency stability analysis in the containment period, different analyses are presented. These analyses have been performed considering system indicators to obtain insight about their effects and the way of their calculation w.r.t. their application in the study of systems with high penetration of power electronic interfaced generation. According to the obtained results, when the level of wind power penetration increases (like GG2020 and GG2030 in GB system) a more radical change from the relationship of ROCOF/NADIR vs. Inertia can be observed. In addition to those indicators, the impacts of the load level and its active power consumption and grid losses, as SMAPD mapping, are also investigated. In this part of the analysis, GB test system has been used for evaluation. According to the findings, the proposed KPI for assessment of the frequency performance in the containment period is based on the mapping of information from the key system variables (inertia, losses and load power) into the well-known indicators (ROCOF/NADIR). Finally, the effect of the FFR of the wind generators on the mapping of ROCOF and NADIR is also discussed and presented. Significant improvement has been achieved after adding FFR capability for frequency control participation of the WGs. These effects become more observable for NADIR due to the type of the FFR controller, and especially for the simulation cases with

highest wind park penetration levels like the GG2030 scenarios in the GB system.

ACKNOWLEDGMENT

This research was carried out as part of the MIGRATE project. This project has received funding from the European Union's Horizon 2020 research and innovation program under grant agreement No 691800. This paper reflects only the authors' views and the European Commission is not responsible for any use that may be made of the information it contains.

REFERENCES

[1] R. Doherty, A. Mullane, G. Nolan, D. J. Burke, A. Bryson, and M. O'Malley, "An assessment of the impact of wind generation on system frequency control," *IEEE Trans. Power Syst.*, vol. 25, no. 1, pp. 452–460, Feb. 2010.

[2] EirGrid and SONI. (2010). *All Island TSO Facilitation of Renewable Studies*. [Online]. Available: http://www.eirgridgroup.com/site-files/library/EirGrid/Facilitation-of-Renewables-Report.pdf

[3] T. Liu, Y. Liu, J. Liu, Y. Yang, G. A. Taylor, and Z. Huang, "Multi-indicator inference scheme for fuzzy assessment of power system transient stability," *CSEE J. Power Energy Syst.*, vol. 2, no. 3, pp. 1–9, Sep. 2016.

[4] R. Preece and J. V. Milanović, "Probabilistic risk assessment of rotor angle instability using fuzzy inference systems," *IEEE Trans. Power Syst.*, vol. 30, no. 4, pp. 1747–1757, Jul. 2015.

[5] S. D. Beigvand, H. Abdi, and S. N. Singh, "Voltage stability analysis in radial smart distribution grids," *IET Gener., Transmiss. Distrib.*, vol. 11, no. 15, pp. 3722–3730, Oct. 2017.

[6] M. Kamel, A. A. Karrar, and A. H. Eltom, "Development and application of a new voltage stability index for on-line monitoring and shedding," *IEEE Trans. Power Syst.*, vol. 33, no. 2, pp. 1231–1241, Mar. 2018.

[7] A. S. Ahmadyar, S. Riaz, G. Verbič, A. Chapman, and D. J. Hill, "A framework for assessing renewable integration limits with respect to frequency performance," *IEEE Trans. Power Syst.*, vol. 33, no. 4, pp. 4444–4453, Jul. 2018.

[8] R. Precup, T. Kamal, and S. Z. Hassan, Eds., "Sensitivity analysis of frequency regulation parameters in power systems with wind generation," in *Advanced Control and Optimization for Wind Energy Systems*. Singapore: Springer, 2019.

[9] J. A. Short, D. G. Infield, and L. L. Freris, "Stabilization of grid frequency through dynamic demand control," *IEEE Trans. Power Syst.*, vol. 22, no. 3, pp. 1284–1293, Aug. 2007.

[10] TenneT. (2016). *MIGRATE Deliverable 1.1: Report on Systemic Issues*. [Online]. Available: https://www.h2020-migrate.eu

[11] J. Morren, S. W. H. de Haan, W. L. Kling, and J. A. Ferreira, "Wind turbines emulating inertia and supporting primary frequency control," *IEEE Trans. Power Syst.*, vol. 21, no. 1, pp. 433–434, Feb. 2006.

[12] P. M. Ashton, C. S. Saunders, G. A. Taylor, A. M. Carter, and M. E. Bradley, "Inertia estimation of the GB power system using synchrophasor measurements," *IEEE Trans. Power Syst.*, vol. 30, no. 2, pp. 701–709, Mar. 2015.

[13] S. Engelken, A. Mendonca, and M. Fischer, "Inertial response with improved variable recovery behaviour provided by type 4 WTs," *IET Renew. Power Gener.*, vol. 11, no. 3, pp. 195–201, Feb. 2017.

[14] E. Rakhshani and P. Rodriguez, "Inertia emulation in AC/DC interconnected power systems using derivative technique considering frequency measurement effects," *IEEE Trans. Power Syst.*, vol. 32, no. 5, pp. 3338–3351, Sep. 2017.

[15] E. Rakhshani, D. Remon, A. M. Cantarellas, J. M. Garcia, and P. Rodriguez, "Virtual synchronous power strategy for multiple HVDC interconnections of multi-area AGC power systems," *IEEE Trans. Power Syst.*, vol. 32, no. 3, pp. 1665–1677, May 2017.

[16] T. S. Borsche, T. Liu, and D. J. Hill, "Effects of rotational inertia on power system damping and frequency transients," in *Proc. 54th IEEE Conf. Decis. Control (CDC)*, Dec. 2015, pp. 5940–5946.

[17] S. S. Guggilam, C. Zhao, E. Dall'Anese, Y. C. Chen, and S. V. Dhople, "Engineering inertial and primary-frequency response for distributed energy resources," Jun. 2017. *arXiv:1706.03612*. [Online]. Available: https://arxiv.org/abs/1706.03612

[18] *Electricity Ten Year Statement, UK Electricity Transmission*, Nat. Grid, London, U.K., Nov. 2016.

[19] DGA Consulting. (2016). *International Review of Frequency Control Adaptation, Australian Energy Market Commission (AEMC)*. [Online]. Available: https://www.aemo.com.au/-/media/Files/Electricity/NEM/Security_and_Reliability/Reports/2016/FPSS—International-Review-of-Frequency-Control.pdf

[20] "Policy 1: Load-frequency control and performance," ENTSO-E, Continental Eur. Oper. Handbook, Tech. Rep., 2018. [Online]. Available: https://www.entsoe.eu/fileadmin/user_upload/_library/publications/entsoe/Operation_Handbook/Policy_1_final.pdf

[21] *Frequency Stability Evaluation Criteria for the Synchronous Zone of Continental Europe*, ENTSO-E, Brussels, Belgium, 2016.

[22] P. Kundur, *Power System Stability And Control*. New York, NY, USA: McGraw-Hill, 1994.

[23] P. Tielens, "Operation and control of power systems with low synchronous inertia," Ph.D. dissertation, Dept. Elect. Eng., Katholieke Univ. Leuven, Leuven, Belgium, Nov. 2017.

[24] U. Rudez and R. Mihalic, "Monitoring the first frequency derivative to improve adaptive underfrequency load-shedding schemes," *IEEE Trans. Power Syst.*, vol. 26, no. 2, pp. 839–846, May 2011.

[25] E. Ørum *et al.* (Nov. 2015). *Future System Inertia*. [Online]. Available: https://docstore.entsoe.eu/Documents/Publications/SOC/Nordic/Nordic_report_Future_System_Inertia.pdf

[26] I. Dudurych, M. Burke, L. Fisher, M. Eager, and K. Kelly, "Operational security challenges and tools for a synchronous power system with high penetration of non-conventional sources," in *Proc. CIGRE Session*, Paris, France, Aug. 2016, pp. 21–26, C2-116.

[27] V. V. Terzija, "Adaptive underfrequency load shedding based on the magnitude of the disturbance estimation," *IEEE Trans. Power Syst.*, vol. 21, no. 3, pp. 1260–1266, Aug. 2006.

[28] L. Ruttledge and D. Flynn, "Short-term frequency response of power systems with high non-synchronous penetration levels," *Wiley Energy Environ.*, vol. 4, no. 5, pp. 452–470, Sep./Oct. 2015.

[29] *Summer Outlook Report*, National Grid Plc, London, U.K., 2018.

[30] H. Chávez, R. Baldick, and S. Sharma, "Governor rate-constrained OPF for primary frequency control adequacy," *IEEE Trans. Power Syst.*, vol. 29, no. 3, pp. 1473–1480, May 2014.

[31] L. Shen, "Model integration and control interaction analysis of AC/VSC HVDC system," Ph.D. dissertation, School Elect. Electron. Eng., Univ. Manchester, Manchester, U.K., 2015.

[32] *Wind Turbines—Part 27-1: Electrical Simulation Models Wind Turbines*, Standard IEC61400-27-1, 2nd ed., 2017.

[33] *MIGRATE Project, Type-3 and Type-4 EMT—Model Documentation*, Energynautics, Darmstadt, Germany, 2017.

[34] EirGRid and SONI. (2011). *DS3: Rate of Change of Frequency (ROCOF) Workstream*. [Online]. Available: http://www.eirgridgroup.com/site-files/library/EirGrid/DS3-Rate-of-Change-of-Frequency-(RoCoF)Workstream-Plan-2011.pdf

[35] E. Rakhshani, D. Remon, and P. Rodriguez, "Effects of PLL and frequency measurements on LFC problem in multi-area HVDC interconnected systems," *Int. J. Elect. Power Energy Syst.*, vol. 81, pp. 140–152, Oct. 2016.

[36] A. E. Leon, J. M. Mauricio, A. Gomez-Exposito, and J. A. Solsona, "Hierarchical wide-area control of power systems including wind farms and FACTS for short-term frequency regulation," *IEEE Trans. Power Syst.*, vol. 27, no. 4, pp. 2084–2092, Nov. 2012.

[37] F. Aminifar, M. Fotuhi-Firuzabad, A. Safdarian, A. Davoudi, and M. Shahidehpour, "Synchrophasor measurement technology in power systems: Panorama and state-of-the-art," *IEEE Access*, vol. 2, pp. 1607–1628, 2014.

[38] S. Jin, Z. Huang, R. Diao, D. Wu, and Y. Chen, "Comparative implementation of high performance computing for power system dynamic simulations," *IEEE Trans. Smart Grid*, vol. 8, no. 3, pp. 1387–1395, May 2017.

[39] E. Rakhshani, J. L. R. Torres, P. Palensky, and M. van der Meijden, "Determination of maximum wind power penetration considering wind turbine fast frequency response," in *Proc. IEEE Milan PowerTech*, Milan, Italy, Jun. 2019, pp. 1–6.

[40] P. Palensky, A. A. Van Der Meer, C. D. Lopez, A. Joseph, and K. Pan, "Cosimulation of intelligent power systems: Fundamentals, software architecture, numerics, and coupling," *IEEE Ind. Electron. Mag.*, vol. 11, no. 1, pp. 34–50, Mar. 2017.

[41] J. L. Rueda, J. C. Cepeda, I. Erlich, A. W. Korai, and F. M. Gonzalez-Longatt, "Probabilistic approach for risk evaluation of oscillatory stability in power systems," in *PowerFactory Applications for Power System Analysis*. Cham, Switzerland: Springer, 2014, pp. 249–266.

[42] P. Teeuwsen, "Oscillatory stability assessment of power systems using computational intelligence," Ph.D. dissertation, Dept. Elect. Eng. Inf. Technol., Univ. Duisburg-Essen, Duisburg, Germany, 2005.

[43] K. Das, J. Hazra, D. P. Seetharam, R. K. Reddi, and A. K. Sinha, "Real-time hybrid state estimation incorporating SCADA and PMU measurements," in *Proc. 3rd IEEE PES Innov. Smart Grid Technol. Eur. (ISGT Europe)*, Oct. 2012, pp. 1–8.

[44] I. Dudurych, J. O'Sullivan, A. Rogers, D. Bell, S. Rourke, and N. Kamalauddin, "Tools for handling high amounts of wind generation in national control centre in Ireland," in *Proc. IEEE Power Energy Soc. Gen. Meeting*, Jul. 2012, pp. 1–8.

ELYAS RAKHSHANI (M'10) was born in 1982. He received the Ph.D. degree *(cum laude)* in electrical engineering from the Technical University of Catalonia (UPC), Barcelona, Spain, in 2016.

From 2013 to 2016, he was with the Research Department, ABENGOA Company, Seville, Spain, as a Junior Researcher, where he was involved in different projects related to power electronics applications and the flexible operation of modern power systems. He is currently a Postdoctoral Researcher with the IEGP Research Center, Delft University of Technology (TU Delft), The Netherlands. In 2017, he joined the IEPG Research Center, where he has been involved in the European H2020 projects related to control and dynamic stability assessment of low-inertia renewable-based power systems. His research interests include power system control and dynamic stability, HVDC control and power converter applications in power systems, wind power integration, frequency control, and optimal intelligent control. Based on his research, he published and presented several scientific works/articles in the most distinguished journals and international conferences in electrical engineering. He has two book chapters, one patent, and several journal articles. He served as a Reviewer for various journals and the IEEE conferences and also served as the Technical Program Committee (TPC) Member for different conferences in the Power and Energy Society (PES).

DIGVIJAY GUSAIN was born in India. He received the master's degree from the Delft University of Technology, in 2016, with a focus on parameter identification of aggregated dynamic load models for active distribution networks, where he is currently pursuing the Ph.D. degree in electrical engineering, with a focus on co-simulation of multi-energy systems. His main research interests include modeling, (co-) simulation, and optimization of energy systems.

VINAY SEWDIEN received the M.Sc. degree *(cum laude)* in electrical engineering from KU Leuven and the Delft University of Technology (TU Delft), in 2013. He is currently pursuing the Ph.D. degree with TU Delft.

After his graduation, he started at TenneT TSO B.V., the Dutch electricity transmission system operator, and worked on topics, such as transparency policies for the electricity industry, wide area measurement systems, and power system stability. He is also a part of the System Operations—International Development Team, where he is investigating the technical implications of the energy transition on the operation of the power system. He is the Technical Secretary of the CIGRE Study Committee C2 on System Operations and Control. Furthermore, he is a member of several CIGRE working groups and the IEEE PES.

JOSÉ L. RUEDA TORRES (SM'12) was born in 1980. He received the Ph.D. degree in electrical engineering from the Universidad Nacional de San Juan, San Juan, Argentina, in 2009. He is currently pursuing the Habilitation (qualification) degree with the Institute of Electrical Power Systems, University of Duisburg-Essen, Essen, Germany. From 2003 to 2005, he worked in Ecuador in the fields of industrial control systems and electrical distribution networks operation and planning. From 2010 to 2014, he was a Postdoctoral Research Associate with the Institute of Electrical Power Systems, University of Duisburg-Essen. He is also an Associate Professor of intelligent electrical power grids with the Department of Electrical Sustainable Energy, Delft University of Technology, Delft, The Netherlands. His research interests include power system stability and control, system identification, power system planning, and probabilistic and artificial intelligence methods. He is the Vice-Chair of the Working Group on Modern Heuristic Optimization (WGMHO) under the IEEE PES Power System Analysis, Computing, and Economics Committee.

MART A. M. M. VAN DER MEIJDEN (M'10) received the M.Sc. degree in electrical engineering from the Technical University of Eindhoven, Eindhoven, The Netherlands, in 1981. From 1982 to 1988, he was with ASEA/ABB in the field of process automation. Since the last 20 years, he has been with different Dutch utilities. He has been involved in development initiatives as grid technology innovation, implementation of sustainable energy, new organizational strategies, and implementation of asset management. Since 2003, he has been with TenneT TSO B.V., as an Innovation Manager, where he is responsible for the development of the TenneT Vision 2030. Since 2011, he has also been a Professor with the Department of Electrical Sustainable Energy, Faculty of Electrical Engineering Mathematics, and Computer Science, Delft University of Technology, Delft, The Netherlands. He has joined and chaired several national and international expert groups.